J. Chem. Sci. Vol. 126, No. 2, March 2014, pp. 511–515.

Determination of conduction and valence band electronic structure of anatase and rutile TiO_2

JAKUB SZLACHETKO[a,b,*], KATARZYNA MICHALOW-MAUKE[b,c], MAARTEN NACHTEGAAL[a] and JACINTO SÁ[a,*]

[a]Paul Scherrer Institute (PSI), 5232 Villigen, Switzerland
[b]Institute of Physics, Jan Kochanowski Unviversity, 25-406 Kielce, Poland
[c]Laboratory for High Performance Ceramics, Empa Swiss Federal Laboratories for Materials Science and Technology, Überlandstrasse 129, 8600 Dübendorf, Switzerland
e-mail: jakub.szlachetko@psi.ch; jacinto.sa@psi.ch

MS received 8 November 2013; revised 24 December 2013; accepted 26 December 2013

Abstract. Electronic structures of rutile and anatase polymorph of TiO_2 were determined by resonant inelastic X-ray scattering measurements and FEFF9.0 calculations. Difference between crystalline structures led to shifts in the rutile Ti *d*-band to lower energy with respect to anatase, i.e., decrease in band gap. Anatase possesses localized states located in the band gap where electrons can be trapped, which are almost absent in the rutile structure. This could well explain the reported longer lifetimes in anatase. It was revealed that HR-XAS is insufficient to study in-depth unoccupied states of investigated materials because it overlooks the shallow traps.

Keywords. Photo-catalysis; high-resolution RIXS; electronic structure.

1. Introduction

Photocatalysis is an emerging field that offers potential to address some of the energy and waste management challenges. $TiO_2$is the most used photocatalyst but requires excitation with UV light due to its wide band gap (anatase ∼3.2 eV; rutile ∼ 3.0 eV). Several methods have been proposed to increase TiO_2 uptake of visible radiation, most notably doping with N, S, C[1] and 3*d* transition metal ions.[2] The improvement relates to direct modification of TiO_2 electronic structure by introduction of in-gap colour centres, i.e., new electronic levels.

Traditional characterization methods such as diffuse reflectance spectroscopy (DRS), allow an indirect estimation of the absorption coefficient and band gap of powder photo-catalysts.[3] However, those techniques provide no information about valence and conduction band electronic structure essential for the rationalization of photocatalytic output. Szlachetko and Sá[4] used a combination of resonant inelastic X-ray scattering (RIXS) and theoretical calculations to determine the electronic structure of undoped anatase TiO_2 and N-doped TiO_2. By combining X-ray emission spectroscopy (XES) and high-resolution X-ray absorption spectroscopy (HR-XAS), they were able to map the electronic structure of occupied and unoccupied states, respectively. In semiconductor terminology, the occupied states corresponds to the valence band, whereas the unoccupied states are related to the conduction band. FEFF calculations of TiO_2 density of states (DOS) revealed that a conduction band is dominated by the empty Ti *d*-band and a valence band is composed of the occupied O *p*-band and Ti *d*-band. Furthermore, accurate determination of the XAS edge positions as a function of doping level enables estimation of the band gap, as previously demonstrated by Chiou *et al.*[5]

Herein, we report the effect that different crystal phases (anatase and rutile) have on electronic structure of TiO_2, determined using RIXS spectroscopy and FEFF calculations as proposed by Szlachetko and Sá.[4] The change in crystalline structure from anatase to rutile leads to a decrease of band gap due to a shift of the Ti *d*-band to lower energy. Anatase possesses localized states located within the band gap, where electrons can be trapped leading to an increase of their lifetime, and availability to react. These states are almost absent in the rutile structure.

2. Experimental

Two commercial TiO_2 powders: anatase (Sigma-Aldrich, SSA_{BET} = 9.55 m^2/g) and rutile (Sigma-Aldrich, SSA_{BET} = 5.75 m^2/g) were investigated. The

*For correspondence

RIXS maps were collected by scanning with 0.5 eV steps around the absorption edge, and recording at each incident energy, the emission spectrum with eV resolution. We used a wavelength dispersive spectrometer operated in the von Hamos geometry.[6] Complete electronic structure of investigated samples was determined by measuring simultaneously the Kβ and valence-to-core transitions around the Ti K-edge. We used a Ge (220) crystal in the von Hamos spectrometer, which provides a relative experimental resolution of 2×10^{-4}. RIXS maps were compared to the theoretical results calculated using the FEFF9.0 code.[7] The code also enabled us to retrieve the orbital constitution for valence and conduction bands for each polymorph. Atoms distribution and arrangement were retrieved from crystal structure of material and used as input file for FEFF9.0 calculations. A cluster with 100 atoms was used for each calculation, and calculation parameters were left unrestricted.

3. Results and discussion

The measured Kβ and v2c RIXS plane for TiO_2 anatase are plotted in figure 1a. For excitation energies above 4980 eV, the RIXS plane consists of the Kβ main emission line resulting from the $3p \rightarrow 1s$ transition at emission energy at around 4933 eV. This Kβ line has some weak spectral structures lying on the high-energy side, which are assigned to the transition of valence electrons to the *1s* core-hole. The diagonal spectral feature crossing the RIXS plane at equal incoming, and emitted X-ray energies relates to the elastically scattered X-rays in the sample. Since the experiments were performed using a dispersive von Hamos spectrometer, which has no moving optical components, the XES spectra are measured on a shot-to-shot basis, and the elastically scattered X-rays allows calibration of the RIXS plane with a precision of about 100 meV. This approach enables analysis of RIXS planes on sample-to-sample basis, and determination of the absolute energies from spectral features/peak positions.

Several aspects can be extracted from the RIXS plane. Firstly, one can extract information on the material's occupied electronic states (valence band) from the non-resonant XES spectrum (figure 1a, top). Three peaks dominate the spectrum, namely the main Kβ emission and two weak structures at energies of 4947 and 4963 eV. Secondly, one can extract information on the material's unoccupied electronic states (conduction band) from the XAS spectrum, which is obtained by integration of the XES counts for each incident X-ray energy.[4]

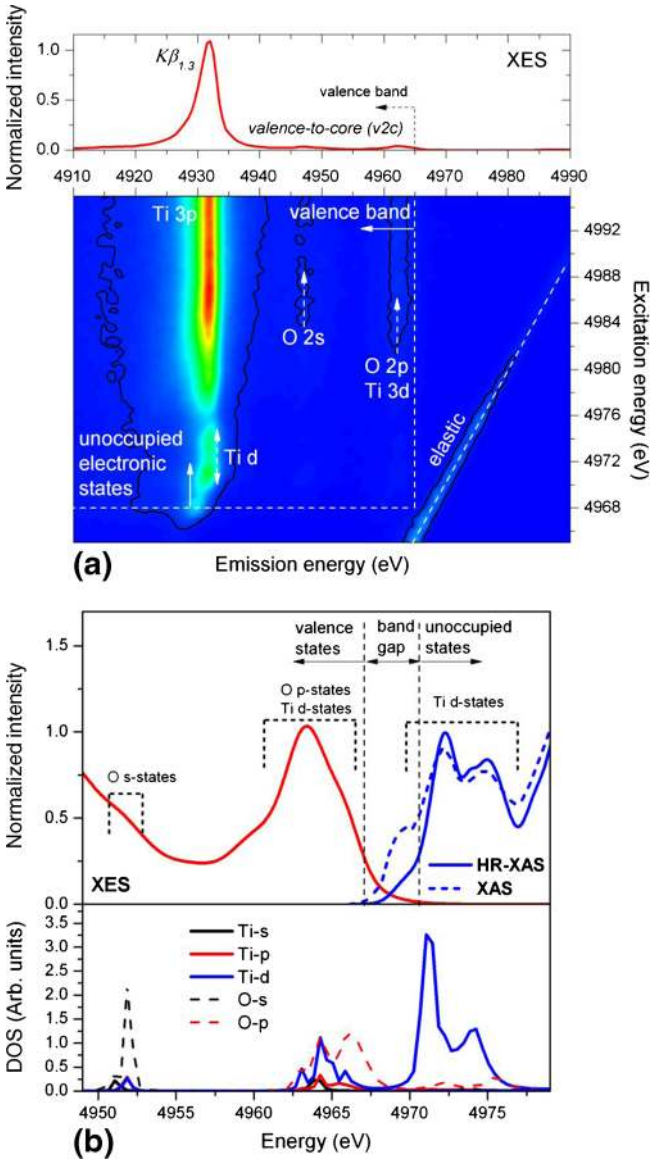

Figure 1. Electronic band structure of TiO_2 anatase. (**a**) RIXS plane with non-resonant XES spectrum (top). (**b**) Valence and conduction band electronic states from RIXS (top) and calculated DOS with FEFF (bottom).

High-resolution XAS (HR-XAS) relates to the cut across the maximum of the Kβ X-ray emission. The resulting XAS (dashed blue line) and HR-XAS (solid blue line) spectra of the pre-edge region are plotted in figure 1b (top). As shown, there are significant differences between XAS and HR-XAS spectra. The XAS spectrum consists of three main features, in agreement with previous experiments,[8,9] while only two peaks are observed in the HR-XAS spectrum. This result implies that the Kβ HR-XAS detection does miss essential parts of the material's unoccupied electronic structure, which might lead to misleading interpretations of the electronic structure.[10]

The presented RIXS experiment relates to the *p*-projected density of states (DOS) of the Ti-site around the Fermi level. Spectral features can be interpreted based on DOS calculations with the FEFF9.0 code.[7] The v2c peak lying just below the Fermi energy consists mostly of Ti-*d* and O-*p* orbitals (figure 1b, bottom). A weak structure in the non-resonant XES spectrum observed at around 4947 eV relates to the O *s*-orbital, which is present at $\sim$ 10–15 eV lower emission energy (i.e., higher binding energy) than the corresponding *p*-orbital. The pre-edge structure is composed mostly of Ti *d*-orbitals. Despite the quadrupolar nature of the $1s \rightarrow d$ excitation (low excitation probability), the pre-edge structures are well-resolved due to *d*- and *p*-orbitals hybridization, leading to a (more intense) dipole-like excitation.[11] The measured occupied (red) and unoccupied (blue) *p*-projected DOS profiles are separated by ca. 3-4 eV, which encompasses TiO_2 band-gap energy. As shown before,[4] the result implies that the RIXS

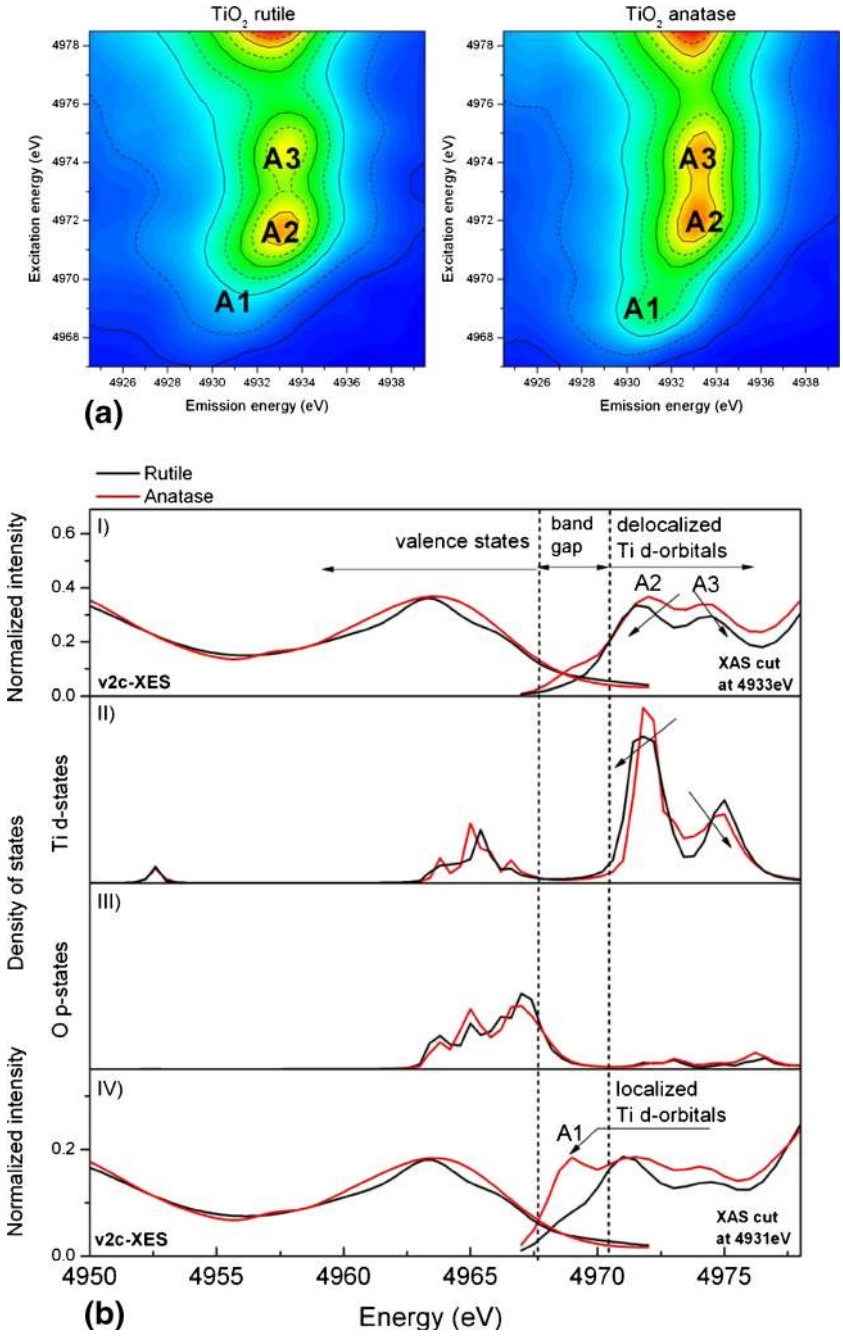

Figure 2. (**a**) Kβ pre-edge RIXS of rutile (left) and anatase (right); (**b**) valence and conduction band states (I) experimental data at 4933 eV; (II) DOS of Ti *d*-orbital; (III) DOS of O *p*-orbital; (IV) experimental data at 4931 eV.

experiment provides band gap-like information, which can be used to analyse samples where commonly used optical methods are insufficient, such as dark samples or samples with strong absorbers (colour centres). However, it should be mentioned that the band gap values estimated with this method are slightly different from the ones obtained by optical spectroscopy due to the electron–electron interaction between the *1s*-excited and valence decaying electron as well as due to core-hole screening effects.

The same RIXS/FEFF strategy was used to establish the differences in electronic structure between TiO_2 in the rutile and anatase phases. The Kβ pre-edge RIXS planes for TiO_2 rutile and anatase are presented in figure 2. The rutile and anatase pre-edge RIXS plane has three main structures. The two main peaks located at excitation energies of 4972 and 4974 eV (both at emission energy of 4933 eV) are due to the excitation of *1s* electron into *3d-4p* hybridized orbital (dipole-like excitation). Due to strong hybridization of *d*- and *p*-orbitals, those *d*-band states are delocalized (A2, A3). These states are sub-bands within the conduction band. The peak at 4969 eV excitation energy (A1) with a lower emission energy ($\sim$ 1.5 eV), is related to the weak *1s-3d* quadrupole transition, i.e., excitation to the localized *d*-orbital.[8,10] We postulate that the localized *d*-orbital states are the so-called shallow traps, located within the band gap. As previously reported,[8] the *3p* state is more affected by *3d*-localized states and thus induces potential difference between *1s3d* and *3p3d* electronic configurations. For this reason, resonance of the *1s*$\rightarrow$*3d*-localized state appears at lower emission energies, which explains its absence in the HR-XAS spectrum compared to XAS (figure 1).

Structures in the RIXS plane of rutile (A2 and A3) have the same origin as that of anatase; however, their intensity and peak positions are different. As shown by FEFF calculations (figure 2b), a slightly larger splitting of the two *3d*-delocalized states is expected for rutile, which was corroborated by the experimental HR-XAS cut at energy of 4933 eV (figure 2b-I). The *3d*-delocalized states splitting for rutile is roughly 0.6 eV (experimental) and 0.4 eV (FEFF calculated); larger than that for anatase. The HR-XAS curves for this emission energy are plotted in figure 2b-IV. In case of anatase, an intense peak was observed in the band gap, while for rutile, only a small shoulder was detected, which is consistent with the proposal that rutile, has very few shallow trap states. Rutile has a shorter distance between the occupied and unoccupied states ($\sim$ 0.2 eV), as expected due to the material's smaller band gap.

4. Conclusion

In conclusion, the presented method enables determination of semiconductor occupied and unoccupied electronic states, i.e., band-gap-like information. To attain exact band gap, one needs to calibrate the maps for titanium scattering factors. However, the strength of the method is not in delivering an exact number for the band gap but in comparing similar materials (e.g., differently doped materials) and to determine what happens to the electronic structure of their bands. For example, in the case of doped materials, one could see the change in valence or conduction or both band structures and estimate energy shifts, which may help rationalize what the dopant is doing. The results shown revealed that the method is sensitive to changes in electronic structure, caused by materials crystal structure. Furthermore, the method is able to resolve localized states in the material (shallow traps). HR-XAS has sharper spectral features and therefore it is often used to gain information about unoccupied states (conduction band). However, this cannot be done without consideration because HR-XAS requires cutting the RIXS map along the most intense emission line, which might miss important features, as demonstrated in this study. Finally, high penetration depth of the X-rays enables study of materials in air and/or under catalytic conditions.

References

1. Asahi R, Morikawa T, Ohwaki T, Aoki K and Taga Y 2001 *Science* **293** 269
2. (a) Carp O, Huisman C L and Reller A 2004 *Prog. Solid State Chem.* **32** 33; (b) Choi J, Park H and Hoffmann M R 2010 *J. Phys. Chem.* **C114** 783; (c) Michalow K, Heel A, Vital A, Amberg M, Fortunato G, Kowalski K, Graule T and Rekas M 2009 *Top. Catal.* **52** 105; (d) Michalow K A, Otal E H, Burnat D, Fortunato G, Emerich H, Ferri D, Heel A and Graule T 2013 *Catal. Today* **209** 47; (e) Michalow K A, Flak D, Heel A, Parlinska-Wojtan M, Graule T and Rekas M 2012 *Environ. Sci. Poll. Res.* **10** 3696
3. (a) Murphy A B 2007 *Sol. Energ. Mat. Sol. Cells* **91** 1326; (b) Michalow K A, Logvinovich D, Weidenkaff A, Amberg M, Fortunato G, Heel A, Graule T and Rekas M 2009 *Catal. Today* **144** 7
4. Szlachetko J and Sá J 2013 *CrystEngComm* **15** 2583

5. Chiou J W, Tsai H M, Pao C W, Chien F Z, Pong W F, Chen C W, Tsai M-H, Wu J J, Ko C H, Chiang H H, Lin H-J, Lee J F and Guo J-H 2008 *J. Appl. Phys.* **104** 013709
6. Szlachetko J, Nachtegaal M, de Boni E, Willimann M, Safonova O V, Sá J, Smolentsev G, Szlachetko M, van Bokhoven J A, Dousse J-Cl, Hoszowska J, Kayser Y, Jagodzinski P, Bergamaschi A, Schmitt B, David C and Lücke A 2012 *Rev. Sci. Instrum.* **83** 103105
7. (a) http://leonardo.phys.washington.edu/feff/; (b) Ankudinov A L, Ravel B, Rehr J J and Conradson S D 1998 *Phys. Rev.* **B58** 7565; (c) Rehr J J and Albers R C 2000 *Rev. Mod. Phys.* **72** 621; (d) Ankudinov A L, Rehr J J, Low J and Bare S R 2001 *Phys. Rev. Lett.* **86** 1642
8. Glatzel P, Sikora M and Fernandez-Garcia M 2009 *Eur. Phys. J.* **169** 207
9. (a) Uozumi T, Okada K, Kotani A, Durmeyer O, Kappler J P, Beaurepaire E, Parlebas, J C 1992 *Europhys. Lett.* **18** 85; (b) Chen L X, Rajh T, Wang Z and Thurnauer M 1997 *J. Phys. Chem.* **B101** 10688; (c) Wu Z Y, Ouvard G, Gressier P and Natoli C R 1997 *Phys. Rev.* **B55** 10382; (d) Wu Z Y, Zhang J, Ibrahim K, Xian D C, Li G, Tao Y, Hu T D, Bellucci S, Marcelli A, Zhang Q H, Gao L and Chen Z Z 2002 *Appl. Phys. Lett.* **80** 2973
10. Carra P, Fabrizio M and Thole B T 1995 *Phys. Rev. Lett.* **74** 3700
11. Frank de Groot 2005 *Coord. Chem. Rev.* **249** 31